Diffusion-driven microstructure evolution in OpenCalphad

Herrnring, Jan; Sundman, Bo; Klusemann, Benjamin

Published in:
Computational Materials Science

DOI:
10.1016/j.commatsci.2019.109236

Publication date:
2020

Document Version
Publisher's PDF, also known as Version of record

Computational Materials Science 175 (2020) 109236

Contents lists available at ScienceDirect

Computational Materials Science

journal homepage: www.elsevier.com/locate/commatsci

Diffusion-driven microstructure evolution in OpenCalphad

Jan Herrnring[a,*], Bo Sundman[b], Benjamin Klusemann[a,c]

[a] Helmholtz-Zentrum Geesthacht, Institute of Materials Research, Max-Planck-Straße 1, 21502 Geesthacht, Germany
[b] OpenCalphad, 9 Allee de l'Acerma, 911 90 Gif sur Yvette, France
[c] Leuphana University of Lüneburg, Institute of Product and Process Innovation, Universitätsallee 1, 21335 Lüneburg, Germany

ARTICLE INFO

Keywords:
Calphad
Bulk diffusion
Mobility
Thermodynamic factor
Precipitation

ABSTRACT

The diffusion process in multicomponent alloys has a significant influence on the evolution of the microstructure. The Calphad approach is a powerful method for describing the equilibrium state as well as the kinetics of non-equilibrium systems via the Gibbs energy. In this work, the principles of multicomponent diffusion theory are considered intensively, and an equation for the fluxes in the case of substitutional-interstitial diffusion is given for implementation. Additionally, the calculation of mobility matrices and thermodynamic factors is addressed. As an application case, substitutional diffusion is implemented in OpenCalphad and is used for calculating the growth rate for spherical precipitates from a supersaturated aluminum matrix. The growth rate has been integrated into the Kampmann–Wagner numerical model, which describes nucleation, growth, and coarsening for spherical precipitates. A AlMgZnCu alloy is considered, which has great significance in the field of materials processing.

1. Introduction

The diffusion process in multicomponent alloys has a considerable influence on microstructure evolution and the mechanical properties resulting from it. In the development of microstructure simulation methods, the Calphad approach is a key method for describing the Gibbs energy and its derived quantities. In general, the phases of the Calphad method are described using solution thermodynamics. The thermodynamic description of the majority of phases is defined by the compound-energy formalism introduced by Sundman and Agren [20]. For a succinct overview of this model, refer to Hillert [11].

In terms of non-equilibrium thermodynamics, the driving force for the diffusion process in a single phase is the minimization of the Gibbs free energy. Depending on the molar Gibbs energy, the favorable energetic state might be achieved by mixing or decomposing atoms. Diffusion in a single phase is typically described by a kinetic equation, representing the flux between lattice planes, and a continuity equation for the conservation of mass. The modeling of kinetic equations has been influenced significantly by the experiment of Kirkendall [13] and the analysis of this phenomenon by Darken [6], which proved that substitutional elements diffuse via a vacancy-exchange mechanism. The important assumptions of Darken's analysis are as follows: (i) a one-dimensional diffusion problem; (ii) conservation of mass; (iii) vacancies are always in thermodynamic equilibrium [3]. However, the assumption of thermodynamic equilibrium should be considered with some caution, because sources and sinks for vacancies are not always directly available in the bulk material.

A multicomponent analysis for modeling diffusion has been proposed by Agren [1] using the compound-energy formalism. Andersson and Agren [2] proposed a phenomenological theory by introducing an optimization approach based on a Redlicher–Kister ansatz for the mobility. This formalism is used in numerous studies for the assessment of mobility databases of various alloy systems such as aluminum–magnesium–zinc [28], iron–manganese–silicon [30], as well as high–entropy alloys [10]. Although the model of Andersson and Agren [2] is often used, it must be noted that the model is not directly applicable to three-dimensional diffusion problems, as shown by Svoboda et al. [25] and Boettinger et al. [4]. Svoboda et al. [25] introduced a diffusion theory based on the thermodynamic extremal principle considering the explicit treatment of vacancies. This approach can be used to consider a complex three-dimensional deformation behavior resulting from mechanical coupling. The explicit treatment of vacancies offers the possibility of taking the derivation from equilibrium directly into account by considering the generation and annihilation mechanisms in the bulk material, as discussed by Fischer et al. [9]. The theory has been recently reviewed by Fischer and Svoboda [8].

In the last decade, considerable efforts have been made by several working groups to integrate the Calphad method in models for the description of solid-state phase transformations. For the phase field method, Zhang et al. [29] recently proposed a model consistent with

* Corresponding author.

https://doi.org/10.1016/j.commatsci.2019.109236
Received 10 May 2019; Received in revised form 7 August 2019; Accepted 27 August 2019
Available online 14 January 2020

the compound-energy formalism. Chen et al. [5] used sharp interface models for the growth and coarsening of spherical precipitates using an ad hoc generalization of the steady-state approximation of the diffusion field. Philippe and Voorhees [18] obtained growth rates by using the steady-state approximation and then used linearization to obtain the growth equations. Kim and Voorhees [12] has extended this work to spheroidal particles in multicomponent alloys. All these models need the full diffusion matrix or at least related quantities for practical application. Here the Calphad method serves as a basis for describing the fluxes of the diffusion process as concentration and temperature dependent via mobilities and the Gibbs energy. In the present work, the kinematic description of Svoboda et al. [23] is used to motivate the transformation formalism proposed by Agren [1]. Thereafter, the model developed by Andersson and Agren [2] is reformulated in terms of diffusion potentials. The reformulation of diffusion potentials allows for a transparent calculation of diffusion coefficients in the open thermodynamic software OpenCalphad[22,21].

The derived formulas have been implemented in OpenCalphad to extend its capabilities to the calculation of mobility matrices, diffusion potentials, as well as the diffusion matrix. As an application of these subroutines, they have been incorporated in a Kampmann–Wagner numerical model describing solid-state precipitation of a quaternary AlCuMgZn alloy.

2. Multicomponent diffusion

In diffusion theory, there is a distinction between the lattice-fixed frame of reference and the volume-fixed frame of reference. Svoboda et al. [25] clarified the definition by using concepts from continuum mechanics. The lattice-fixed frame of reference corresponds to the actual configuration, whereas the laboratory-fixed frame of reference corresponds to the reference configuration. In the following, the treatment of Svoboda et al. [23] is summarized, and additionally, their notation is slightly adjusted to be consistent with the nomenclature commonly used in the compound-energy formalism. First, a relation for the total flux J_k, resulting from the diffusive flux of elements j_k relative to the lattice in the actual configuration and the Kirkendall velocity, is derived. Then the theory outlined by Svoboda et al. [23] is used to clarify the underlying assumptions of the transformation formalism utilized by Andersson and Agren [2].

2.1. Phase structure and kinematic description

In diffusion theory, there is a general distinction between substitutional and interstitial diffusion. According to Hillert [11], an interstitial sublattice is characterized by a low-site fraction of atoms and a high-site fraction of vacancies. The substitutional elements typically form the crystal lattice, whereas the interstitial elements fill the voids within the lattice. From this definition, it follows that the diffusion process for interstitial elements is quite different from the diffusion process of substitutional elements. For elements on an interstitial lattice, a jump to an adjacent lattice site should be possible because the next lattice site is empty. In contrast to the diffusion mechanism of interstitial elements, elements on a substitutional sublattice diffuse via a vacancy-exchange mechanism. The jump of an atom to the next lattice site is thus only possible if a vacancy is available in the neighborhood of the element. Since the fraction of vacant lattice sites is low, the diffusion process for substitutional elements is significantly slower than for interstitial elements.

In this treatment, a phase consisting of a substitutional and an interstitial sublattice is considered. This assumption leads to the following phase structure: $(S_0, S_1, ..., S_n)_a\ (I_{n+1}, ..., I_{n+m}, Va)_b$ for a phase comprising substitutional elements S_k, $k \in [0, n]$ as well as interstitial elements I_k, $k \in [n+1, n+m]$. Here S_0 denotes the vacancies belonging to the substitutional sublattice. Va describes the vacancies of the interstitial sublattice. The stoichiometric coefficients belonging to their respective sublattices are denoted by a and b. In the following, a volume element containing $\mathfrak{N}^\alpha$ moles per formula unit of phase α is considered. The index α is not considered in the following discussion because diffusion considers only a single phase. For reasons of clarity, the site fractions of the substitutional sublattice are denoted by y_k^1, $k \in [0, n]$ and interstitial elements are denoted by y_k^2, $k \in [n+1, n+m]$. As usual, the site fractions are restricted by

$$\sum_{i=0}^{n} y_i^1 = 1 \quad \text{and} \quad \sum_{i=n+1}^{n+m} y_i^2 + y_{Va}^2 = 1. \tag{2.1}$$

Based on the compound-energy formalism, the number of moles N_k contained in the volume element is calculated by

$$\begin{aligned} N_k &= \mathfrak{N} a y_k^1 \quad \text{for} \quad k \in [1, n]; \\ N_k &= \mathfrak{N} b y_k^2 \quad \text{for} \quad k \in [n+1, n+m]. \end{aligned} \tag{2.2}$$

The mole fractions in the volume element are calculated by

$$\begin{aligned} x_k &= \frac{a y_k^1}{a[1 - y_{Va}^1] + b[1 - y_{Va}^2]} \quad \text{for} \quad k \in [1, n] \quad \text{or} \\ x_k &= \frac{b y_k^2}{a[1 - y_{Va}^1] + b[1 - y_{Va}^2]} \quad \text{for} \quad k \in [n+1, n+m]. \end{aligned} \tag{2.3}$$

The total number of lattice sites is

$$N = \mathfrak{N}[a + b]. \tag{2.4}$$

The number of moles N contained in the reference volume is a non-conservative variable because vacancies can be generated or annihilated at vacancy sources or sinks. The generation or annihilation in the considered volume and the diffusion process leads to volumetric changes. The volume of the reference element W is described by using partial molar volumes Ω_k, which do not depend on the composition by assumption

$$W = \sum_{k=0}^{n+m} N_k \Omega_k. \tag{2.5}$$

The volume related to a single mole of substitutional elements is introduced by

$$\bar{\Omega} = \frac{W}{N_S} \quad \text{with} \quad N_S = \sum_{k=0}^{n} N_k = \sum_{k=0}^{n} \mathfrak{N} a y_k^1 = \mathfrak{N} a. \tag{2.6}$$

The previous definitions allow expressing the volume W of the reference element via u-fractions, which has been introduced earlier by Andersson and Agren [2]:

$$\bar{\Omega} = \sum_{k=0}^{n+m} u_k \Omega_k \quad \text{with} \quad u_k = \frac{N_k}{N_S}. \tag{2.7}$$

In diffusion theory, it is helpful to use u-fractions under certain assumptions. The conversion between fractions u_k and site fractions y_k is followed by invoking Eqs. (2.2) and (2.6) into the definition of the u-fraction given in Eq. (2.7):

$$\begin{aligned} u_k &= y_k^1 \quad \text{for} \quad k \in [0, n]; \\ u_k &= \tfrac{b}{a} y_k^2 \quad \text{for} \quad k \in \{[n+1, n+m], Va\}. \end{aligned} \tag{2.8}$$

The definition of the partial molar volume for vacancies Ω_0 on the substitutional sublattice is not trivial. Here the formula developed by Svoboda et al. [23] is used to ensure a consistent treatment of volume changes by working with

$$\bar{\Omega}_0 = \sum_{k=1}^{n} \frac{u_k \Omega_k}{1 - u_0}. \tag{2.9}$$

The volume of the volume element W is then described by

$$W = u_0 \bar{\Omega}_0 + \sum_{k=1}^{n+m} N_k \Omega_k. \tag{2.10}$$

Invoking Eq. (2.9) into Eq. (2.7) reveals for the molar volume $\bar{\Omega}$, with reference to a single mole of substitutional elements, the following expression:

$$\bar{\Omega} = u_0\bar{\Omega}_0 + \sum_{k=1}^{n+m} u_k\Omega_k = u_0\sum_{k=1}^{n}\frac{u_k\Omega_k}{1-u_0} + \sum_{k=1}^{n}\Omega_k u_k + \sum_{k=n+1}^{n+m} u_k\Omega_k \tag{2.11}$$

$$= \left[\frac{u_0}{1-u_0}+1\right]\sum_{k=1}^{n} u_k\Omega_k + \sum_{n+1}^{n+m} u_k\Omega_k$$

$$= \frac{1}{1-u_0}\sum_{k=1}^{n} u_k\Omega_k + \sum_{n+1}^{n+m} u_k\Omega_k. \tag{2.12}$$

The volume related to a single mole of substitutional elements can be set in relation to the molar volume. This can be achieved by considering the definition of the molar volume and using the definition of the u-fraction and Eq. (2.12)

$$\Omega = \frac{\sum_{k=0}^{n+m} N_k\Omega_k}{\sum_{k=1}^{n+m} N_k} = \frac{\sum_{k=0}^{n+m} u_k\Omega_k}{\sum_{k=1}^{n+m} u_k} = \frac{\bar{\Omega}}{\sum_{k=1}^{n+m} u_k}. \tag{2.13}$$

It follows from this equation that the molar volume is generally not a constant and depends on the fractions for the vacancies on each sublattice. Eqs. (2.1), (2.3),(2.8), and (2.13) can be used to show that the following relationship holds for the concentration c_k

$$c_k = \frac{x_k}{\Omega} = \frac{u_k}{\bar{\Omega}}. \tag{2.14}$$

Following the introduction of the essential composition variables, it is necessary to consider the vacancy-exchange mechanism. If the rate of jumps of the elements between the lattice planes is not identical, this introduces a movement of the substitutional lattice sites. The net flux of elements across a lattice plane must be balanced by vacancies moving in the opposite direction. This net flux of elements leads to a local movement of the lattice; it is denoted by velocity $\vec{v}$ and gets its name from its discoverer Ernest Kirkendall—the Kirkendall effect.

In the following, it is shown how an expression for the Kirkendall velocity $\vec{v}$ can be derived. According to standard continuum mechanics [7], the rate of change in an arbitrary volume element is related to the divergence of the velocity $\vec{v}$ of that volume element by

$$\mathrm{div}(\vec{v}) = \frac{\dot{W}}{W}. \tag{2.15}$$

The right-hand side of Eq. (2.15) is further analyzed using the product rule

$$\frac{\dot{W}}{W} = \frac{\dot{\bar{\Omega}}N_S + \dot{N}_S\bar{\Omega}}{\bar{\Omega}N_S} = \frac{\dot{\bar{\Omega}}}{\bar{\Omega}} + \frac{\dot{N}_S}{N_S}. \tag{2.16}$$

Here it is necessary to derive a relationship for the rate of $\dot{\bar{\Omega}}$. This is achieved by analyzing flux balances for each individual element. To this end, a flux balance at the boundary ∂V of the volume element is considered:

$$\dot{N}_k = -\int_{\partial V}\vec{j}_k\cdot\vec{m}\,ds = -\int_V \mathrm{div}(\vec{j}_k)dv \quad \text{for} \quad k = 1,\ldots,n+m. \tag{2.17}$$

Here the divergence theorem has been applied. According to Svoboda et al. [25,23], local averaging and using Eq. (2.6) lead to

$$\frac{\dot{N}_k}{N_S} = -\bar{\Omega}\,\mathrm{div}(\vec{j}_k) \quad \text{for} \quad k = 1,\ldots,n+m. \tag{2.18}$$

Owing to the Kirkendall effect, substitutional atoms diffuse by a vacancy-exchange mechanism, and the flux of elements is balanced by the flux of vacancies:

$$\sum_{k=1}^{n}\vec{j}_k = -\vec{j}_0. \tag{2.19}$$

The balance equation for the vacancies follows from Eq. (2.18) by a summation of overall substitutional elements and usage of Eq. (2.19)

$$\frac{\dot{N}_0}{N_S} = -\bar{\Omega}\,\mathrm{div}(\vec{j}_0) + \frac{\dot{N}_S}{N_S}. \tag{2.20}$$

Recalling the assumption that the partial molar volumes of the individual components are constant, and using the quotient rule for determining the rate of $\bar{\Omega}$ from Eq. (2.12), we get:

$$\dot{\bar{\Omega}} = \sum_{k=1}^{n}\Omega_k\frac{\dot{u}_k[1-u_0]+u_k\dot{u}_0}{[1-u_0]^2} + \sum_{k=n+1}^{n+m}\dot{u}_k\Omega_k. \tag{2.21}$$

As shown by Svoboda et al. [23], the resulting u-fraction rates $\dot{u}_k$ in Eq. (2.21) are obtained by a differentiation of Eq. (2.8) in combination with Eq. (2.18)

$$\dot{u}_k = \frac{\dot{N}_k}{N_S} - \frac{N_k\dot{N}_S}{N_S^2} = -\bar{\Omega}\mathrm{div}(\vec{j}_k) - u_k\frac{\dot{N}_S}{N_S} \quad \text{for} \quad k = [1,\, n+m]. \tag{2.22}$$

The rate of the u-fraction for the vacancies is obtained by

$$\dot{u}_0 = \frac{\dot{N}_0}{N_S} - \frac{N_0\dot{N}_S}{N_S^2} = -\bar{\Omega}\,\mathrm{div}(\vec{j}_0) + \frac{\dot{N}_S}{N_S}(1-u_0). \tag{2.23}$$

If the creation or annihilation of vacancies is assumed to be infinitely fast, then the concentration of vacancies is identical to the equilibrium concentration, and $\dot{u}_0$ equals zero. Svoboda et al. [23] deduced from Eq. (2.23) the following relation if creation or annihilation of vacancies is infinitely fast:

$$\frac{\dot{N}_S}{N_S} = \frac{\bar{\Omega}}{[1-u_0^{eq}]}\mathrm{div}(\vec{j}_0). \tag{2.24}$$

Svoboda et al. [23] derived the following equation for the right-hand side of Eq. (2.15) by combining Eqs. (2.22) and (2.23) with Eq. (2.21). The obtained expression for $\dot{\bar{\Omega}}$ is set into Eq. (2.16) and results after the collection of terms in

$$\frac{\dot{W}}{W} = \frac{\dot{N}_S}{N_S}\frac{\bar{\Omega}_0}{\bar{\Omega}} - \left[\sum_{k=1}^{n}\frac{(\Omega_k-\bar{\Omega}_0)\mathrm{div}(\vec{j}_k)}{1-u_0} + \sum_{k=n+1}^{n+m}\Omega_k\mathrm{div}(j_k)\right]. \tag{2.25}$$

Instead of using u-fractions, it is common to describe the evolution equations in terms of concentrations. As shown by Fischer and Svoboda [8], Eq. (2.22) can be reformulated in terms of concentrations by replacing $u_k = c_k\bar{\Omega}$ in accordance with Eq. (2.14). After using the product rule, rearranging, and dividing by $\bar{\Omega}$, the following formula results from Eqs. (2.22):

$$\dot{c_k} = -\mathrm{div}(\vec{j}_k) - \left[\frac{\dot{N}_S}{N_S} - \frac{\dot{\bar{\Omega}}}{\bar{\Omega}}\right]c_k. \tag{2.26}$$

Using Eqs. (2.15) in combination with (2.16) leads to

$$\dot{c}_k = -\mathrm{div}(\vec{j}_k) - \mathrm{div}(\vec{v})c_k. \tag{2.27}$$

The rate of change in a concentration $\dot{c}_k$ is a material derivative

$$\frac{Dc_k}{Dt} = \frac{\partial c_k}{\partial t} + \vec{v}\cdot\nabla c_k. \tag{2.28}$$

Combining Eqs. (2.27) and (2.28) yields

$$\frac{\partial c_k}{\partial t} = -\vec{v}\cdot\nabla c_k - c_k\mathrm{div}(\vec{v}) - \mathrm{div}(\vec{j}_k) = -\mathrm{div}(\vec{j}_k + c_k\vec{v}). \tag{2.29}$$

Hence, the total flux is a combination of the intrinsic fluxes and an additional flux resulting from the Kirkendall effect:

$$\vec{J}_k = \vec{j}_k + c_k\vec{v}. \tag{2.30}$$

An often-applied approximation is to assume that the u-fraction for substitutional vacancies u_0 can be neglected and the generation of vacancies is infinitely fast. This assumption is of great importance in practice because the equilibrium u-fraction, or equivalently the site

fraction of vacancies on the substitutional sublattice, is seldom described explicitly because of its small magnitude. Invoking Eqs. (2.19) and (2.24) into Eq. (2.25), and using the approximation that the equilibrium u-fraction of vacancies is negligible: $u_0^{eq} \approx 0$, lead to

$$\mathrm{div}(\vec{v}) = -\sum_{k=1}^{n+m} \Omega_k \mathrm{div}(\vec{j_k}). \tag{2.31}$$

If the variation of concentrations is considered only in one dimension, the integration of Eq. (2.31) is simplified significantly to

$$v = -\sum_{k=1}^{n+m} \Omega_k j_k \tag{2.32}$$

as pointed out by Svoboda et al. [23]. By combining Eqs. (2.14), (2.30), and (2.32), the total flux is determined:

$$J_k = j_k + v\,c_k = j_k - \frac{x_k}{\Omega}\sum_{i=1}^{n+m} \Omega_i j_i. \tag{2.33}$$

The total flux given in Eq. (2.33) corresponds to the form used by Agren [1]

$$J_k = \sum_{i=1}^{n+m} L_{ik}{}' j_i, \quad L_{ik}{}' = \left[\delta_{ik} - x_k \frac{\Omega_i}{\Omega}\right]. \tag{2.34}$$

In the following, it is assumed that the fraction of vacancies is negligible and in local equilibrium.

2.2. Evolution equations

The multicomponent diffusion theory considered here is based on Onsager's force flux relation [16]. The driving forces for diffusion are identified with the negative gradients of the chemical potentials $-\frac{\partial \mu_k}{\partial z}$ of component k, multiplied by phenomenological coefficients L_{ki} and resulting in the following formula for intrinsic fluxes:

$$j_k = -\sum_{i=1}^{n+m} L_{ki} \frac{\partial \mu_i}{\partial z}. \tag{2.35}$$

The coefficients L_{ki} must be symmetric to fulfill Onsager's reciprocity relation. However, the chemical potentials used in Eq. (2.35) are not independent as they are related via the Gibbs–Duhem relation:

$$\sum_{i=1}^{n+m} x_i \frac{\partial \mu_i}{\partial z} = 0. \tag{2.36}$$

Agren [1] recommended a procedure for obtaining independent driving forces for diffusion:

$$j_k = -\sum_{i=1}^{n+m} L_{ki}{}' \left[\frac{\partial \mu_i}{\partial z} - \frac{\partial \mu_r}{\partial z}\right], \quad \text{with} \quad L_{ki}{}' = \sum_{j=1}^{n+m} \left[\delta_{ij} - x_i \frac{\Omega_j}{\Omega}\right] L_{kj}. \tag{2.37}$$

For an arbitrary substitutional element r belonging to the substation sublattice, a combination of Eq. (2.34) and Eq.(2.37) yields

$$J_k = -\sum_{i=1}^{n+m} L''_{ki} \left[\frac{\partial \mu_i}{\partial z} - \frac{\Omega_i}{\Omega_r}\frac{\partial \mu_r}{\partial z}\right] \quad \text{with}$$
$$L''_{ki} = \sum_{r=1}^{n+m}\sum_{j=1}^{n+m} \left[\delta_{ir} - x_i \frac{\Omega_r}{\Omega}\right]\left[\delta_{jk} - x_k \frac{\Omega_j}{\Omega}\right] L_{jr}. \tag{2.38}$$

In the following, based on Andersson and Agren [2], it is assumed that all elements of the substitutional sublattice have the constant partial molar volume Ω_S, i.e. $\Omega_i = \Omega_S$ for all elements $i \in [1, n]$ when Ω_i denotes the partial molar volume corresponding to mole fraction x_i of element i. Elements of the interstitial sublattice do not contribute to the molar volume, hence $\Omega_i = 0$, $\forall\ i \in [n+1, n+m]$. By using this assumption, the evaluation of Eq. (2.38) is simplified significantly. Moreover, based on Eq. (2.14), it follows that

$$x_k \frac{\Omega_j}{\Omega} = u_k \quad \text{for} \quad j \in [1, n] \quad \text{or}$$
$$x_k \frac{\Omega_j}{\Omega} = 0 \quad \text{for} \quad j \in [n+1, n+m]. \tag{2.39}$$

Considering that element r is contained in the substitutional sublattice, Eq. (2.38) is expanded for the flux to

$$J_k = -\sum_{i=1}^{n+m} L''_{ki} \frac{\partial}{\partial z}\left[\mu_i - \frac{\Omega_i}{\Omega_r}\mu_r\right] = -\sum_{i=1}^{n} L''_{ki} \frac{\partial}{\partial z}[\mu_i - \mu_r] - \sum_{i=n+1}^{n+m} L''_{ki} \frac{\partial \mu_i}{\partial z}. \tag{2.40}$$

The fluxes of element k are now split according to substitutional and interstitial elements. Andersson and Agren [2] used the following ansatz for the flux in the lattice-fixed frame of reference:

$$j_k = -c_k M_k \frac{\partial \mu_k}{\partial z} \quad \text{if} \quad k \in [1, n] \quad \text{or}$$
$$j_k = -c_k y_{Va}^2 M_k \frac{\partial \mu_k}{\partial z} \quad \text{if} \quad k \in [n+1, n+m] \tag{2.41}$$

using the mobility coefficients M_k. Based on this modeling approach, the following cases are valid:

$$L_{kk} = c_k M_k \quad \text{if} \quad k \in [1, n] \quad \text{or} \quad L_{kk} = c_k y_{Va} M_k \quad \text{if} \quad k \in [n+1, n+m] \quad \text{else} \quad L_{kj} = 0. \tag{2.42}$$

An expansion of Eq. (2.38) facilitates the simplification of the coefficients

$$L''_{ki} = \sum_{r=1}^{n}\sum_{j=1}^{n} \left[\delta_{ir} - x_i \frac{\Omega_r}{\Omega_m}\right]\left[\delta_{jk} - x_k \frac{\Omega_j}{\Omega_m}\right] L_{jr} + \sum_{r=1}^{n}\sum_{j=n+1}^{n+m} [\cdots] + \sum_{r=n+1}^{n+m}\sum_{j=1}^{n} [\cdots] + \sum_{r=n+1}^{n+m}\sum_{j=n+1}^{n+m} [\cdots] \tag{2.43}$$

$$= \sum_{j=1}^{n}\sum_{r=1}^{n} [\delta_{jk}\delta_{ir} - \delta_{jk}u_i - \delta_{ir}u_k + u_k u_i] L_{jr} + \sum_{r=n+1}^{n+m}\sum_{j=n+1}^{n+m} \delta_{ir}\delta_{jk} L_{jr}. \tag{2.44}$$

The second as well as the third summation is zero due to the definition of L_{jr} based on Eq. (2.42). Therefore, the summation can be simplified for the possible element combinations:

- if $k \in [1, n]$ and $i \in [1, n]$ and $k = i$

$$L''_{kk} = [1 - 2u_k] L_{kk} + u_k^2 \sum_{j=1}^{n} L_{jj}, \tag{2.45}$$

- if $k \in [1, n]$ and $i \in [1, n]$ and $k \neq i$

$$L''_{ki} = -u_k L_{ii} - u_i L_{kk} - u_i u_k \sum_{j=1}^{n} L_{jj}, \tag{2.46}$$

- if $k \in [1, n]$ and $i \in [n+1, n+m]$

$$L''_{ki} = -u_i L_{kk} + u_i u_k \sum_{j=1}^{n} L_{jj}, \tag{2.47}$$

- if $k \in [n+1, n+m]$ and $i \in [1, n]$

$$L''_{ki} = -u_k L_{ii} + u_i u_k \sum_{j=1}^{n} L_{jj}, \tag{2.48}$$

- if $k \in [n+1, n+m]$ and $i \in [n+1, n+m]$ and $k \neq i$

$$L''_{ki} = u_i u_k \sum_{j=1}^{n} L_{jj}, \tag{2.49}$$

- if $k \in [n+1, n+m]$ and $i \in [n+1, n+m]$ and $k = i$

$$L''_{ki} = u_i u_k \sum_{j=1}^{n} L_{jj} + L_{ii}. \tag{2.50}$$

Since it is usually not practical to directly evaluate the gradients of chemical potentials, it is necessary to further manipulate Eq. (2.40). For phases with sublattices, it is not always possible to directly calculate the chemical potential for each component, but the partial Gibbs energies of the end-members can always be determined. End-members denote the limiting case where only one species is present in every sublattice. As outlined in detail by Sundman et al. [22], the chemical potentials are related to the partial Gibbs energy of the end-member. The possible end-members form compounds with defined stoichiometry, and all possible end-members can be determined by the permutation of the species occurring on different sublattices. The partial Gibbs energy of the end-member is generally determined for an end-member tuple I by

$$G_I = G_M + \sum_s \left(\frac{\partial G_M}{\partial y^s_{i\in I}}\right)_{T,P,y_{j\neq i}} - \sum_s \sum_j y^s_j \left(\frac{\partial G_M}{\partial y^s_j}\right)_{T,P,y_{k\neq j}}. \tag{2.51}$$

Due to the considered phase structure, it is possible to evaluate the chemical potentials of the substitutional and interstitial sublattices with the same kind of formalism based on Eq. (2.51). The assumption that vacancies are in a thermal equilibrium makes the following manipulations possible for an end-member tuple $\{k\colon Va\}$

$$G_{k:Va} = a\mu_k + b\mu_{Va} = a\mu_k \rightarrow \mu^1_k - \mu^1_r = \frac{1}{a}[G_{k:Va} - G_{r:Va}]. \tag{2.52}$$

Using Eq. (2.51) and Eq. (2.52) results in

$$\mu_k - \mu_r = \frac{1}{a}\left[\frac{\partial G_M}{\partial y^1_k} - \frac{\partial G_M}{\partial y^1_r}\right] \quad \text{for} \quad k \in [1, n],\ r \in [1, n]. \tag{2.53}$$

For interstitial elements, similar manipulations give

$$\mu_k = \tfrac{1}{b}[G_{s:k} - G_{s:Va}] = \tfrac{1}{b}\left[\tfrac{\partial G_M}{\partial y^2_k} - \tfrac{\partial G_M}{\partial y^2_{Va}}\right] \quad \text{for} \quad s \in [1, n],\ k \in [n+1, n+m]. \tag{2.54}$$

The application of the chain rule to Eq. (2.53) leads to

$$\frac{\partial}{\partial z}[\mu_k - \mu_r] = \frac{1}{a}\sum_{j=1}^{n}\left[\frac{\partial^2 G_M}{\partial y^1_j \partial y^1_k} - \frac{\partial^2 G_M}{\partial y^1_j \partial y^1_r}\right]\frac{\partial y^1_j}{\partial z}. \tag{2.55}$$

Eq. (2.40) is transformed into a suitable form for computational tasks by using Eqs. (2.53)–(2.55):

$$\begin{aligned} J_k &= -\sum_{i=1}^{n} L''_{ki}\tfrac{\partial}{\partial z}[\mu^1_i - \mu^1_r] - \sum_{i=n+1}^{n+m} L''_{ki}\tfrac{\partial \mu^2_i}{\partial z} \\ &= -\tfrac{1}{a}\sum_{i=1}^{n} L''_{ki}\sum_{j=1}^{n}\left[\tfrac{\partial^2 G_M}{\partial y^1_j \partial y^1_i} - \tfrac{\partial^2 G_M}{\partial y^1_j \partial y^1_r}\right]\tfrac{\partial y^1_j}{\partial z} \\ &\quad -\tfrac{1}{b}\sum_{i=n+1}^{n+m} L''_{ki}\sum_{j=n+1}^{n+m}\left[\tfrac{\partial^2 G_M}{\partial y^2_j \partial y^2_i} - \tfrac{\partial^2 G_M}{\partial y^2_j \partial y^2_{Va}}\right]\tfrac{\partial y^2_j}{\partial z}. \end{aligned} \tag{2.56}$$

In the next section, the flux is rewritten with regard to diffusion constants for substitutional elements. Manipulations on the interstitial sublattice can be performed accordingly.

2.3. Diffusion of a substitutional sublattice

If only substitutional elements form the phase, the second term of Eq. (2.56) vanishes. Since it is common to eliminate the dependent site fraction y^1_r by accounting for the restriction given in Eq. (2.1), the following relation is obtained by

$$J_k = -\frac{1}{a}\sum_{i=1}^{n} L''_{ki}\sum_{j=1\backslash r}^{n}\phi_{ij}\frac{\partial y^1_j}{\partial z} \quad \text{with}$$
$$\phi_{ij} = \left[\frac{\partial^2 G_M}{\partial y^1_j \partial y^1_i} - \frac{\partial^2 G_M}{\partial y^1_r \partial y^1_i} - \frac{\partial^2 G_M}{\partial y^1_j \partial y^1_r} + \frac{\partial^2 G_M}{\partial y^1_r \partial y^1_r}\right], \tag{2.57}$$

where $j = 1\backslash r$ means summation of all substitutional elements except r. The derivation of Eq. (2.57) is shown in detail in the Appendix. The quantity ϕ_{ij} corresponds to the Hessian of the molar free energy and is also a key quantity for the recent sharp interface phase transformation models, cf. Philippe and Voorhees [18] and Kim and Voorhees [12]. Diffusion coefficients for a substitutional alloy can be calculated by a comparison with the relation for the fluxes given in Eq. (2.57):

$$J_k = -\frac{1}{a}\sum_{j\neq r} D^r_{kj}\frac{\partial c_j}{\partial z}, \quad k \neq r, \tag{2.58}$$

$$J_k = -\frac{1}{a}\sum_{i=1}^{n} L''_{ki}\frac{\partial}{\partial z}[\mu^1_i - \mu^1_r] = -\frac{\Omega}{a}\sum_{i=1\backslash r}^{n}\sum_{i=1\backslash r}^{n} L''_{ki}\phi_{ij}\frac{\partial c_j}{\partial z}, \tag{2.59}$$

$$D^r_{kj} = \frac{\Omega}{a}\sum_{i=1\backslash r}^{n} L''_{ki}\phi_{ij}. \tag{2.60}$$

Interestingly, $L_{ki}{}''$ and ϕ_{ij} are symmetric; however, this does not imply that the diffusion matrix is symmetric. The first term is often denoted as mobility matrix $L_{ki}{}''$ and the second term is considered a thermodynamic factor ϕ_{ij}, e.g. [18,12]. The coefficients of the mobility matrix, see also Eqs. (2.45)–(2.50), are calculated for the case $k = i$ by

$$L''_{kk} = [1 - 2x_k]L_{kk} + x_k^2\sum_j L_{jj}. \tag{2.61}$$

If $k \neq i$ the coefficients are calculated by

$$L''_{ki} = -x_k L_{ii} - x_i L_{kk} - x_i x_k \sum_j L_{jj}. \tag{2.62}$$

The L_{kk} factor is defined by

$$L_{kk} = c_k M_k = \frac{x_k}{\Omega}M_k, \tag{2.63}$$

This shows that the diffusion does not depend on Ω for substitutional phases and reassembles the equations given by Agren [1]. The description of the mobility coefficients is done according to Yao et al. [28], using a frequency factor and activation energy Φ_i

$$M_i = \frac{1}{R_{gas}T}\exp\left(\frac{\Phi_i}{R_{gas}T}\right) \quad \text{with} \quad \Phi_i = \sum_p x_p Q_i^p + \sum_p\sum_{q>p} x_p x_q \sum_k^k Q_i^{p,q}[x_p - x_q]^k. \tag{2.64}$$

Here, the exponent k determines the order of the Redlicher–Kister polynomial. R_{gas} and T denote the gas constant and the temperature, respectively. Q_i^p are the coefficients of the Redlicher–Kister polynomial. To sum up the previous discussion, to calculate the diffusion matrix, a thermodynamic database is necessary to determine the thermodynamic factor. Additionally, a diffusion database is necessary to obtain the mobility matrix. In this work, a routine for the calculation of interdiffusion matrices has been implemented in OpenCalphad. The open thermodynamic and diffusion databases from Matcalc for aluminum are used to obtain the interdiffusion coefficients at 725 K for a ternary aluminum–magnesium–zinc alloys. The numerical results are compared with experimental results from Takahashi et al. [26] and plotted on a Gibbs triangle in Fig. 1. The used diffusion database is based on the assessment of Yao et al. [28]. As discussed by Yao et al. [28], the simulated cross-diffusion coefficients are negative and significantly smaller than the diagonal diffusion coefficients. Figs. 1 (b) and (c) show negative cross-diffusion coefficients with more significant derivations from the experiments. However, Yao et al. [28] noticed similar features for the cross-diffusion coefficients and argued that the measurement of cross-diffusion coefficients is a delicate topic.

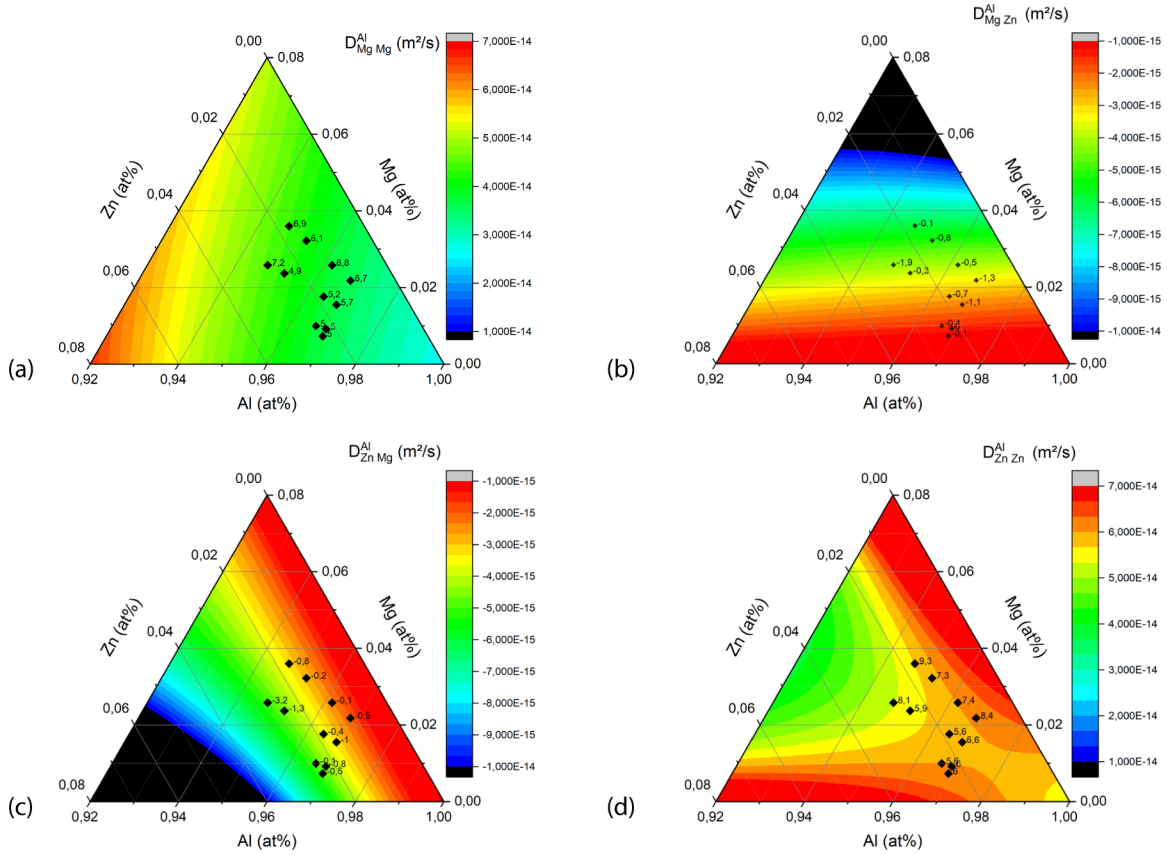

Fig. 1. Interdiffusion coefficients of the ternary aluminum–magnesium–zinc system at 725 K. The marked points are experimental determined diffusion constants from Takahashi et al. [26]. The experimental values are given in 10^{-14} m^2/s.: (a) $D^{Al}_{Mg,Mg}$. (b) $D^{Al}_{Mg,Zn}$(c) $D^{Al}_{Zn,Mg}$ (d) $D^{Al}_{Zn,Zn}$.

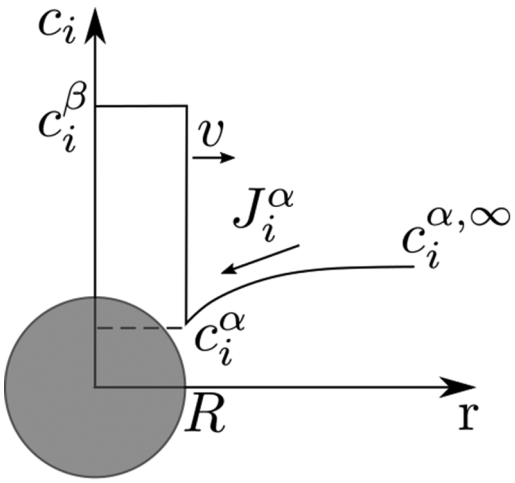

Fig. 2. Growth of a spherical precipitate β in a supersaturated matrix α [14].

3. Solid-state precipitation

3.1. Sharp interface model

Sharp interface models are an important tool in material science for describing solid-state phase transformations. Typically, sharp interface models determine the growth rates for spherical or prolate ellipsoidal precipitates in a matrix phase via semi-analytic approaches. Often a flux balance is established between the matrix phase and the precipitate phase. The equations from the previous section are used for determining the diffusive fluxes in the matrix phase. The velocity of the precipitate matrix interface v, which describes the growth or dissolution rate of a precipitate in a matrix, is an important quantity in the Kampmann–Wagner numerical model, which describes phase transformations via a discrete particle-density distribution function.

In the following, the invariant field method as discussed by Philippe and Voorhees [18] is used. In contrast to Philippe and Voorhees [18], in this contribution the introduced linearization is avoided, and the discussion thus ends in a nonlinear system of equations. It should be noted that this approach is closely related to the method proposed by Chen et al. [5].

For reasons of completeness, a short derivation of the necessary nonlinear equation system for obtaining the growth rate is discussed. In the following, a stoichiometric spherical precipitate of phase β with radius R is considered in an infinite matrix phase α, as shown in Fig. 2. The concentrations of the precipitate and the matrix are denoted by c_i^α and c_i^β, respectively. The far-field concentration of the matrix is denoted by $c_i^{\alpha,\infty}$. If the partial molar volumes for every element are assumed to be similar, the flux balance at the precipitate–matrix interface for each independent concentration c_j must hold separately. The first component is chosen arbitrarily as the dependent component. Philippe and Voorhees [18] set up the following flux balance at the precipitate matrix interface for a spherical precipitate by considering cross diffusion.

$$[x_j^\beta - x_j^\alpha]v = \sum_{k=2}^{n} D^1_{jk}\frac{\partial x_k}{\partial r}\Big|_{r=R}, \quad j = 2, \ldots, n. \tag{3.65}$$

In contrast to Philippe and Voorhees [18], the flux balance according to Eq. (3.65) is written in terms of mole fractions x_j. This is because this quantity is more convenient to use in a Calphad framework. The next step is the calculation of the concentration profile in the matrix phase using the solution of the diffusion equation in spherical coordinates. By applying the invariant field approximation, the

transient term of the diffusion equation is neglected. The application of an eigenvalue–eigenvector decomposition as outlined by Vermolen et al. [27] leads to the solution provided by Philippe and Voorhees [18] for the mole fraction x_j^α in phase α:

$$x_j^\alpha = x_j^{\alpha,\infty} + [x_j^\alpha - x_j^{\alpha,\infty}]\frac{R}{r} \quad j = 2, \ldots, n. \tag{3.66}$$

The flux balance for the invariant field approximation results from the combination of Eq. (3.65) and Eq. (3.66).

$$[x_j^\beta - x_j^\alpha]v = \sum_{k=2}^{n} \frac{D_{jk}^1 [x_k^{\alpha,\infty} - x_k^\alpha]}{R}, \quad j = 2, \ldots, n. \tag{3.67}$$

Since a stoichiometric precipitate is assumed, there are n-1 equations for unknown n provided by Eq. (2.19). To close the system of equations, an additional relation is necessary. This relation is obtained by applying the local equilibrium assumption at the precipitate matrix interface:

$$\mu_i^\alpha = \mu_i^\beta, + \frac{2\sigma\,\Omega_i}{R}, \quad i = 1, \ldots, n. \tag{3.68}$$

If particular stoichiometric precipitates are considered, then the chemical potentials cannot be evaluated as the variation of the concentration is forbidden by definition. In this case, the relation between the molar Gibbs energy G_m and the chemical potentials has to be used for closing the non-linear system of equations:

$$G_m^\beta = \sum_i^n x_i^\beta \mu_i^\beta = \sum_i^n x_i^\beta \left[\mu_i^\alpha - \frac{2\,\Omega_i \sigma}{R}\right]. \tag{3.69}$$

The definition of partial molar quantities facilitates the simplification of Eq. (3.69). By using the molar volume Ω for the β-phase and the interfacial energy σ, the following equation is derived for stoichiometric precipitates:

$$G_m^\beta + \frac{2\sigma\,\Omega}{R} = \sum_i^n x_i^\beta \mu_i^\alpha. \tag{3.70}$$

The combination of Eqs. (3.67) and (3.70) is the Calphad-consistent generalization of the commonly used solubility product formalism often used in solid-state phase transformations, as outlined by Perez et al. [17], among others. To use Eq. (3.67), the diffusion matrix has been calculated as discussed in the previous section. The dependency of the diffusion matrix has been accounted for by using the far-field concentration of the matrix phase.

3.2. Kampmann–Wagner model

The Kampmann–Wagner model describes the nucleation, growth, and coarsening of a dispersion of spheres in a unit volume by a particle-density distribution function f. The particle-density distribution function f obeys a continuity equation in the size space as shown by Ratke and Voorhees [19]:

$$\frac{\partial f}{\partial t} + \frac{\partial}{\partial R}(fv) = j. \tag{3.71}$$

In this case, v is the growth or dissolution rate of a spherical particle, as determined in the previous subsection, and j is the density distribution of nucleated particles. The number of particles in the unit volume n_V, mean radius $\bar{R}$, and the volume fraction f_p are derived from the particle-density distribution function by the evaluation of the zero, first, and third moment, respectively:

$$n_V = \int_0^\infty f dR, \quad \bar{r} = \frac{\int_0^\infty R f dR,}{n_V}, \quad f_p = \frac{4\pi}{3}\int_0^\infty R^3 f dR. \tag{3.72}$$

The mole fractions in the far field of the matrix $x_i^{\alpha,\infty}$ are calculated from the mean mole fractions of the alloy x_i^0 and the volume fraction f_p by

$$x_i^{\alpha,\infty} = \frac{x_i^0 - f_p x_i^\beta}{1 - f_p}. \tag{3.73}$$

The source term is calculated by employing a multicomponent extension of classic nucleation theory according to Svoboda et al. [24]:

$$I = N Z \beta^* \exp\left(-\frac{16\pi}{3}\frac{\sigma^3\Omega^2}{[d_{chem}^{\alpha\mapsto\beta}]^2}\right), \tag{3.74}$$

using the Zeldovic factor Z and the atomic attachment rate β^*. The potential number of nucleation sites N is approximated by the Avogadro constant divided by the molar volume. The quantity $d_{chem}^{\alpha\mapsto\beta}/\Omega$ in Eq. (3.74) describes the volumetric energy that is released when an infinitesimal volume of α-phase is transformed into the β-phase. The Zeldovic factor Z and the atomic attachment rate β^* are calculated as follows:

$$Z = \frac{a_L^6}{64\pi^2 k_B T}\frac{[d_{chem}^{\alpha\mapsto\beta}]^4}{[\Omega]^4\sigma^3} \quad \text{and} \quad \beta^* = \frac{4\pi R_c^2}{a_L^4}\left[\sum_{i=1}^{n}\frac{[x_i^\beta - x_i^\alpha]^2}{x_i^\alpha D_i^{Tracer}}\right]^{-1} \tag{3.75}$$

using the mean interatomic distance a_L, the Boltzmann constant k_B, and the tracer diffusion coefficient D_i^{Tracer}. The tracer diffusion coefficient is calculated by $D_i^{Tracer} = R_{gas}\,T\,M_i$, where the mobility coefficients M_i are determined by Eq. (2.64). Classic nucleation theory predicts the creation of a particle around the critical radius R_c with a certain size spectrum. According to Ratke and Voorhees [19], the nucleation rate I is connected to the source term of the particle-density distribution j by

$$I = \int_{R_c}^\infty j\,dr. \tag{3.76}$$

The critical radius R_c is determined by solving the equation system resulting from Eqs. (3.67) and (3.69) with $v = 0$. The source term j of the hyperbolic partial differential Eq. (3.71) is described in this work by a normed Gaussian distribution function that is unequal to zero in the interval $[R_c, R_c + \Delta R^N]$. The limitation of j is achieved by using the Heaviside function $H(\bullet)$ via

$$j(R,t) = \frac{2I}{\sqrt{\pi}\,\xi_e}\frac{[H(R-R_c) - H(R-[R_c+\Delta R^N])]}{\mathrm{erf}\left(\frac{\Delta R^N}{\xi_e}\right)}\exp\left(-\left[\frac{R-R_c}{\xi_e}\right]^2\right), \tag{3.77}$$

where ξ_e is a constant and ΔR^N is the length of the interval, where the source term in Eq. (3.71) is not zero. The condition expressed in Eq. (3.76) is fulfilled via normalization, resulting in the given prefactor of Eq. (3.77). The solution of the hyperbolic partial differential Eq. (3.71) is achieved with a multi-class approach. The particle-density distribution function is discretized by a high-resolution finite volume method with a minmod flux-limiter, as discussed by LeVeque [15]. The implemented numerical scheme is followed by dividing the radius space in finite volumes of size $[R_{i-1/2}, R_{i+1/2}]$, as illustrated in Fig. 3. For the sake of simplicity, it is assumed that the discretization is realized by a uniform grid. In Fig. 3, $v_{i-1/2}$ denotes the velocity at the boundary of cell i with $R_{i-1/2}$. The integration of Eq. (3.71) over the domain $[R_{i-1/2}, R_{i+1/2}] \times [t_n, t_{n+1}]$ yields

$$\begin{aligned}&\int_{t_n}^{t_{n+1}}\int_{R_{i-1/2}}^{R_{i+1/2}}\frac{\partial f}{\partial t}dR dt + \int_{t_n}^{t_{n+1}}\int_{R_{i-1/2}}^{R_{i+1/2}}\frac{\partial}{\partial R}[fv]\,dR\,dt\\ &= \int_{t_n}^{t_{n+1}}\int_{R_{i-1/2}}^{R_{i+1/2}} j\,dR\,dt.\end{aligned} \tag{3.78}$$

Using the fundamental theorem of calculus results in

$$\begin{aligned}&\int_{r_{i-1/2}}^{r_{i+1/2}}\left[\frac{\partial f}{\partial t}(r, t_{n+1}) - \frac{\partial f}{\partial t}(r, t_n)\right]dr + \int_{t_n}^{t_{n+1}}[f(r_{i+1/2}, t)v(r_{i+1/2}, t)\\ &\quad - f(r_{i-1/2}, t)v(r_{i-1/2}, t)]\,dr\,dt = \int_{t_n}^{t_{n+1}}\int_{r_{i-1/2}}^{r_{i+1/2}} j\,dr\,dt.\end{aligned} \tag{3.79}$$

The average value of the particle-density distribution function $\overline{N}_i^n$, the average value of the particle-density distribution of nucleated

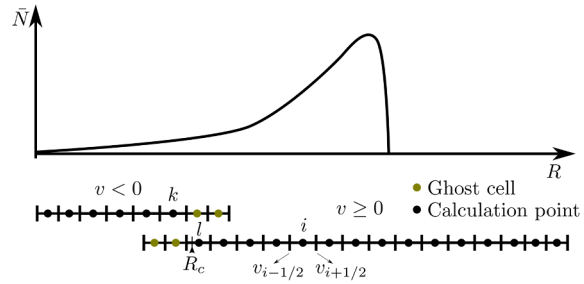

Fig. 3. Schematic discretization of the radius space into finite volumes for solving Eq. (3.71). The radius space is divided in every time step into two size classes—one for dissolving precipitates ($v < 0$) and the other for growing precipitates $v \geqslant 0$.

particles $\bar{S}_i^n$ in the interval $\Delta R_i = R_{i+1/2} - R_{i-1/2}$, and the flux $F_{i+1/2}^n$ are defined by

$$\begin{aligned}
\bar{N}_i^n &= \frac{1}{\Delta R_i}\int_{R_{i-1/2}}^{R_{i+1/2}} f(R, t_n)dR,\\
\bar{S}_i^n &= \frac{1}{\Delta R_i}\int_{R_{i-1/2}}^{R_{i+1/2}} j(R, t_n)dR. \quad \text{and}\\
\bar{F}_{i+1/2}^n &= \frac{1}{\Delta t}\int_{t_n}^{t_{n+1}} f(R_{i+1/2}, t)v(R_{i+1/2}, t)dt.
\end{aligned} \tag{3.80}$$

Based on this definition, Eq. (3.79) is rearranged to

$$\bar{N}_i^{n+1} = \bar{N}_i^n + \frac{\Delta t}{\Delta R_i}[F_{i-1/2}^n - F_{i+1/2}^n] + \bar{S}_i^n \Delta t. \tag{3.81}$$

Here the source term is approximated by an explicit Euler scheme. The fluxes at the boundaries of the finite volumes are calculated for a uniform grid using the following definition:

$$\delta_{i-1/2} = \begin{cases} 1 & v_{i-1/2} \geqslant 0 \\ -1 & v_{i-1/2} < 0. \end{cases} \tag{3.82}$$

Then the flux $F_{i-1/2}$ at the boundary $i - 1/2$ of the finite volume can be calculated as

$$\begin{aligned}
F_{i-1/2} = {} & \tfrac{1}{2}v_{i-1/2}[(1 + \delta_{i-1/2})\bar{N}_{i-1}^n + (1 - \delta_{i-1/2})\bar{N}_i^n]\\
& + \tfrac{1}{2}|v_{i-1/2}|\left(1 - \left|\tfrac{v_{i-1/2}\Delta t}{\Delta r}\right|\right)\phi(\kappa_{i-1/2}^n)[\bar{N}_i^n - \bar{N}_{i-1}^n].
\end{aligned} \tag{3.83}$$

Here a flux-limiter $\kappa_{i-1/2}^n$ is used to avoid oscillations:

$$\kappa_{i-1/2}^n = \begin{cases} \frac{\bar{N}_{i-1}^n - \bar{N}_{i-2}^n}{\bar{N}_i^n - \bar{N}_{i-1}^n} & v_{i-1/2} \geqslant 0 \\ \frac{\bar{N}_{i+1}^n - \bar{N}_i^n}{\bar{N}_i^n - \bar{N}_{i-1}^n} & v_{i-1/2} < 0 \end{cases} \tag{3.84}$$

in combination with a superbee flux-limiter function $\phi(\kappa) = max(0, min(1, 2\kappa), min(2, \kappa))$. The resulting scheme for solving the particle-density distribution function is second-order accurate in R in smooth parts of the solution and is reduced to first-order accurate at discontinuities. For the used time step, the Courant–Friedrichs–Lewy condition must be fulfilled. From Eqs. (3.81)–(3.84), it follows that, instead of solving the average particle-density distribution function $\bar{N}_i^{n+1}$, it can be solved equivalently for the particles $N_i^{n+1} = \bar{N}_i^{n+1}\Delta R_i$, which are contained in ΔR_i. For implementation purposes, it is convenient to use this property and has been used by Perez et al. [17]. The high-resolution finite volume scheme must be used with some care because the flux-limiter needs information from the upwind direction. According to Fig. 3, the particle-distribution function is separated in radius-space into two size classes. The first size class contains all cells whose boundaries are smaller than the critical radius R_c. This size class handles precipitates that dissolve. The second size class starts with the first cell, whose left boundary is smaller than or equal to the critical radius and contains all size classes that represent growing precipitates. With reference to Fig. 3, it must be assured that the fluxes $F_{k+1/2}$ and $F_{l-1/2}$ vanish because otherwise particles would be created artificially. This is achieved by adding ghost cells with a zero value as shown in Fig. 3.

The described Kampmann–Wagner numerical model is used to describe nucleation, growth, and coarsening of an alloy system consisting of $X_{Cu}^0 = 0.54\%$, $X_{Mg}^0 = 3.6\%$, $X_{ZN}^0 = 3.33\%$. In the calculations, a temperature of 443.15 K and an interfacial energy σ of 0.105 J/m^2 have been assumed. The velocity v, which corresponds to growth or dissolution in the radius space, is plotted for different radii and volume fractions f_p in Fig. 4(a). Naturally, different volume fractions result in different matrix concentrations. The matrix concentrations enter into Eq. (3.67), thereby directly influencing the velocity v. In Fig. 4(a), the stoichiometric η'-phase of the open Matcalc aluminum database is considered. It is obvious that growth depends significantly on the volume fraction f_p. The growth velocity corresponding to low volume fractions is significantly higher than the velocity for higher volume fractions. Hence, if the volume fraction deviates significantly from the equilibrium during the nucleation and growth stages, the velocity is considerably higher as in the region of coarsening. Additionally, it is obvious that dissolution is a faster process than growth.

The evolution of the volume fraction is more intensively investigated in Fig. 4(b). Here a normed volume fraction $\bar{f}_p$ is used, referring to the equilibrium volume fraction. The equilibrium volume fraction for the η'-phase is 5.29% and the fraction reached finally in the simulation, as shown in Fig. 4(b) after $t > 10^6$ seconds, is 5.19%. Fig. 5(a) shows the evolution of the number of particles and the mean radius. It indicates that the nucleation and growth-time regime reaches approximately 10^4 seconds. After this regime, the precipitation process reaches the transient region, where the volume fraction and mean

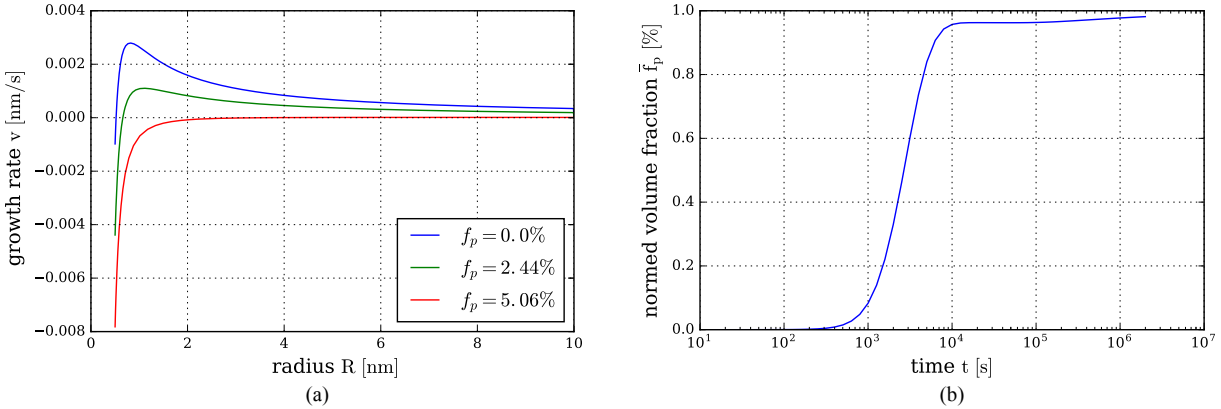

Fig. 4. (a) Growth velocity for the η' phase for different precipitate volume fractions f_p at 443.15 K and a composition of $X_{Cu}^0 = 0.54\%$, $X_{Mg}^0 = 3.6\%$, $X_{ZN}^0 = 3.33\%$. (a) Velocity for different radii. (b) Evolution of normed volume fraction $\bar{f}_p$ of η' phase predicted by the Kampmann–Wagner numerical model.

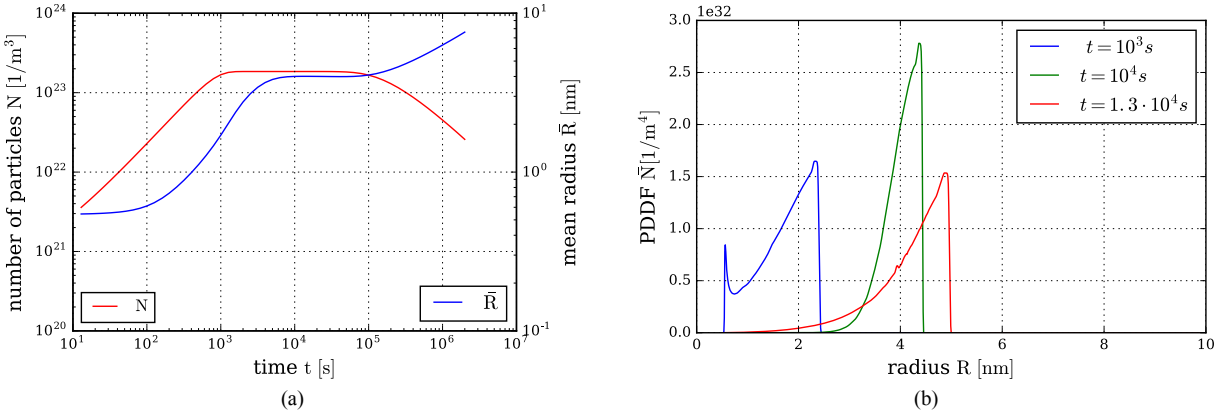

Fig. 5. Results from Kampmann–Wagner numerical model: (a) evolution of the number of particles N and the mean radius $\bar{r}$; (b) particle density distribution function (PDDF) at different times.

Table 1
(a) Interdiffusion coefficients for a matrix composition associated with a vanishing volume fraction $\boldsymbol{D}^{Al,f_P=0.0\%}$, (b) Interdiffusion matrix for a volume fraction corresponding to a matrix composition resulting from a volume fraction of 5.09% $\boldsymbol{D}^{Al,f_P=5.09\%}$. Interdiffusion coefficients are given in m^2/s.

$$\begin{bmatrix} 1.5852\cdot10^{-20} & -1.3820\cdot10^{-21} & -6.5068\cdot10^{-21} \\ 1.2064\cdot10^{-21} & 2.9207\cdot10^{-19} & -6.2429\cdot10^{-20} \\ -1.5233\cdot10^{-20} & -3.7930\cdot10^{-20} & 1.4344\cdot10^{-19} \end{bmatrix}$$

(a)

$$\begin{bmatrix} 3.8665\cdot10^{-20} & -5.8529\cdot10^{-22} & -1.4374\cdot10^{-21} \\ 4.7528\cdot10^{-22} & 1.6957\cdot10^{-19} & -2.8521\cdot10^{-20} \\ -1.8943\cdot10^{-21} & -6.1266\cdot10^{-21} & 2.0721\cdot10^{-19} \end{bmatrix}$$

(b)

radius remain almost constant. The coarsening starts approximately at $5\cdot10^4$ seconds, where the mean radius and the volume fraction begin to increase again, whereas the number of particles decreases. In order to complete the discussion, the particle-density distribution function is shown in Fig. 5(b) for different times.

Another interesting question is which changes occur in the interdiffusion matrix during the simulation. In Table 1, the interdiffusion matrix is considered for the case of total dissolution of precipitates and a volume fraction close to equilibrium. It is interesting to note that the diffusion constants on the diagonal change significantly. The coefficient $D^{Al}_{Mg,Mg}$ decreases significantly, whereas the other main coefficients increase. However, in the transient region and during coarsening the volume fraction changes only slightly; therefore, the diffusion matrix is almost constant.

4. Conclusion

A consistent method for the calculation of fluxes, mobilities, and thermodynamic factors has been discussed and the underlying assumptions outlined based on the diffusion model introduced by Andersson and Agren [2]. The model has been reformulated in terms of diffusion potentials and implemented into OpenCalphad. Using an in-depth discussion of the model structure, the authors hope to clarify the foundations of that method. These quantities are of great significance in many practical applications, and the integration in codes for diffusion processes is a natural next step. In this work, the method for determining diffusion coefficients is coupled with a sharp interface model. The growth rates calculated from the sharp interface model are used as an input into a multicomponent Kampmann–Wagner numerical model. As shown by the work, OpenCalphad can serve as a rich source of important input for recent microstructure simulation models.

5. Data availability

The thermodynamic and diffusion databases required to reproduce these findings can be downloaded from https://matcalc.at/. The software used to reproduce these findings will be made available to download from https://www.opencalphad.com/.

CRediT authorship contribution statement

Jan Herrnring: Conceptualization, Methodology, Software, Writing - original draft, Writing - review & editing. **Bo Sundman:** Software, Writing - review & editing. **Benjamin Klusemann:** Writing - review & editing, Funding acquisition.

Acknowledgement

Irmela Burkhardt and Martin Frönd are kindly acknowledged for their advice for the preparation of the ternary plots. The authors confirm that there are no known conflicts of interest related to this publication, and that there has been no significant financial support for this work that could have influenced its outcome.

Appendix A

This appendix discusses the derivation of the diffusion potential introduced by Agren [1]. The first term of Eq. (2.56) is

$$-\frac{1}{a}\sum_{i=1}^{n} L''_{ki}\left[\sum_{j=1\backslash r}^{n}\left[\frac{\partial^2 G_M}{\partial y_j^1 \partial y_i^1}-\frac{\partial^2 G_M}{\partial y_j^1 \partial y_r^1}\right]\frac{\partial y_j^1}{\partial z}+\left[\frac{\partial^2 G_M}{\partial y_r^1 \partial y_i^1}-\frac{\partial^2 G_M}{\partial y_r^1 \partial y_r^1}\right]\frac{\partial y_r^1}{\partial z}\right]. \tag{A.1}$$

From the restriction given in Eq. (2.1), it follows

$$\frac{\partial y_r^1}{\partial z} = -\sum_{j=1\backslash r}^{n} \frac{\partial y_j^1}{\partial z}. \tag{A.2}$$

Then Eq. (A.1) can be reformulated into

$$-\frac{1}{a}\sum_{i=1}^{n} L''_{ki}\left[\sum_{j=1\backslash r}^{n}\left[\frac{\partial^2 G_M}{\partial y_j^1 \partial y_i^1} - \frac{\partial^2 G_M}{\partial y_j^1 \partial y_r^1}\right]\frac{\partial y_j^1}{\partial z} - \left[\frac{\partial^2 G_M}{\partial y_r^1 \partial y_i^1} - \frac{\partial^2 G_M}{\partial y_r^1 \partial y_r^1}\right]\sum_{j=1\backslash r}^{n}\frac{\partial y_j^1}{\partial z}\right]. \tag{A.3}$$

Collecting terms leads to the expression given in Eq. (2.57)

$$-\frac{1}{a}\sum_{i=1}^{n} L''_{ki}\sum_{j=1\backslash r}^{n}\left[\frac{\partial^2 G_M}{\partial y_j^1 \partial y_i^1} - \frac{\partial^2 G_M}{\partial y_j^1 \partial y_r^1} - \frac{\partial^2 G_M}{\partial y_r^1 \partial y_i^1} + \frac{\partial^2 G_M}{\partial y_r^1 \partial y_r^1}\right]\frac{\partial y_j^1}{\partial z}. \tag{A.4}$$

References

[1] J. Agren, Diffusion in phases with several components and sublattices, J. Phys. Chem. Solids 43 (5) (1982) 421–430.
[2] J.-O. Andersson, J. Agren, Models for numerical treatment of multicomponent diffusion in simple phases, J. Appl. Phys. 72 (4) (1992) 1350–1355.
[3] R.W. Balluffi, S. Allen, W.C. Carter, Kinetics of Materials, John Wiley & Sons, 2005.
[4] W. Boettinger, J. Guyer, C. Campbell, G. McFadden, Computation of the kirkendall velocity and displacement fields in a one-dimensional binary diffusion couple with a moving interface, Proc. R. Soc. A 463 (2007) 3347–3373 12.
[5] Q. Chen, J. Jeppsson, J. Agren, Analytical treatment of diffusion during precipitate growth in multicomponent systems, Acta Mater. 56 (8) (2008) 1890–1896.
[6] L. Darken, Diffusion, mobility and their interrelation through free energy in binary metallic systems, Trans. Metall. Soc. AIME 175 (1948) 184ff.
[7] E.A. de Souza Neto, D. Peric, D. Owen, Computational Methods for Plasticity: Theory and Applications, John Wiley & Sons, 2011.
[8] F. Fischer, J. Svoboda, Diffusion of elements and vacancies in multi-component systems, Prog. Mater Sci. 60 (2014) 338–367.
[9] F. Fischer, J. Svoboda, F. Appel, E. Kozeschnik, Modeling of excess vacancy annihilation at different types of sinks, Acta Mater. 59 (9) (2011) 3463–3472.
[10] D. Gaertner, K. Abrahams, J. Kottke, V.A. Esin, I. Steinbach, G. Wilde, S.V. Divinski, Concentration-dependent atomic mobilities in fcc cocrfemnni high-entropy alloys, Acta Mater. 166 (2019) 357–370.
[11] M. Hillert, The compound energy formalism, J. Alloy. Compd. 320 (2) (2001) 161–176.
[12] K. Kim, P.W. Voorhees, Ostwald ripening of spheroidal particles in multicomponent alloys, Acta Mater. 152 (2018) 327–337.
[13] E.O. Kirkendall, Diffusion of zinc in alpha brass, Trans. AIME 147 (1942) 104–110.
[14] E. Kozeschnik, Modeling Solid-state Precipitation, Momentum press, 2013.
[15] LeVeque, R.J., 2002. Finite volume methods for hyperbolic problems. Vol. 31. Cambridge University Press.
[16] L. Onsager, Reciprocal relations in irreversible processes. ii, Phys. Rev. 38 (12) (1931) 2265.
[17] M. Perez, M. Dumont, D. Acevedo-Reyes, Implementation of classical nucleation and growth theories for precipitation, Acta Mater. 56 (9) (2008) 2119–2132.
[18] T. Philippe, P. Voorhees, Ostwald ripening in multicomponent alloys, Acta Mater. 61 (11) (2013) 4237–4244.
[19] L. Ratke, P.W. Voorhees, Growth and Coarsening: Ostwald Ripening in Material Processing, Springer Science & Business Media, 2002.
[20] B. Sundman, J. Agren, A regular solution model for phases with several components and sublattices, suitable for computer applications, J. Phys. Chem. Solids 42 (4) (1981) 297–301.
[21] B. Sundman, U.R. Kattner, C. Sigli, M. Stratmann, R.L. Tellier, M. Palumbo, S.G. Fries, The opencalphad thermodynamic software interface, Comput. Mater. Sci. 125 (2016) 188–196.
[22] B. Sundman, X.-G. Lu, H. Ohtani, The implementation of an algorithm to calculate thermodynamic equilibria for multi-component systems with non-ideal phases in a free software, Comput. Mater. Sci. 101 (2015) 127–137.
[23] J. Svoboda, F. Fischer, P. Fratzl, Diffusion and creep in multi-component alloys with non-ideal sources and sinks for vacancies, Acta Mater. 54 (11) (2006) 3043–3053.
[24] J. Svoboda, F. Fischer, P. Fratzl, E. Kozeschnik, Modelling of kinetics in multi-component multi-phase systems with spherical precipitates: I: Theory, Mater. Sci. Eng.: A 385 (1) (2004) 166–174.
[25] J. Svoboda, F. Fischer, P. Fratzl, A. Kroupa, Diffusion in multi-component systems with no or dense sources and sinks for vacancies, Acta Mater. 50 (6) (2002) 1369–1381.
[26] T. Takahashi, Y. Minamino, T. Yamane, Quaternary diffusion in 7000 aluminum alloys, Mater. Trans. 43 (2) (2002) 232–238.
[27] F. Vermolen, K. Vuik, S. van der Zwaag, The dissolution of a stoichiometric second phase in ternary alloys: a numerical analysis, Mater. Sci. Eng.: A 246 (1–2) (1998) 93–103.
[28] J. Yao, Y.-W. Cui, H. Liu, H. Kou, J. Li, L. Zhou, Diffusional mobility for fcc phase of al-mg-zn system and its applications, Calphad 32 (3) (2008) 602–607.
[29] L. Zhang, M. Stratmann, Y. Du, B. Sundman, I. Steinbach, Incorporating the calphad sublattice approach of ordering into the phase-field model with finite interface dissipation, Acta Mater. 88 (2015) 156–169.
[30] W. Zheng, X.-G. Lu, Y. He, Y. Cui, L. Li, Thermodynamic assessment of the fe-mn-si system and atomic mobility of its fcc phase, J. Alloy. Compd. 632 (2015) 661–675.